Journal of Materials Chemistry A

PAPER

View Article Online
View Journal | View Issue

Cite this: J. Mater. Chem. A, 2014, 2, 13905

Improving the photovoltaic performance of ladder-type dithienonaphthalene-containing copolymers through structural isomerization†

Yunlong Ma, Qingdong Zheng,* Lixin Wang, Dongdong Cai, Changquan Tang, Meng Wang, Zhigang Yin and Shan-Ci Chen

A ladder-type angular-shaped dithienonaphthalene (**aDTN**), an isomer of ladder-type linear-shaped dithienonaphthalene (**DTN**), was designed and synthesized as an electron-rich unit to construct donor–acceptor copolymers with deep-lying highest occupied molecular orbital (HOMO) energy levels. Benzo[*c*][1,2,5]thiadiazole (**BT**) with various substituents were used as electron deficient units for synthesizing the target copolymers (**PaDTNBTO**, **PaDTNBTH**, and **PaDTNBTF**) *via* the Stille coupling reaction. Incorporating different substituents onto the **BT** moiety has significant effects on the photophysical and electrochemical properties of the copolymers, as well as on the roughness of the polymer/$PC_{71}BM$ blends. With four solubilizing alkyl chains on the **aDTN** unit, all its three copolymers have good solubility in common solvents. The synthesized copolymers exhibit deep-lying HOMO energy levels, leading to high open circuit voltages ($V_{oc} \geq 0.90$ V) of the resulting polymer solar cells. The bulk heterojunction solar cell based on the **aDTN**-containing copolymers (**PaDTNBTO**) shows an improved efficiency of 6.44% and an increased V_{oc} of 0.92 V compared to that based on the linear-shaped **DTN** containing counterpart (efficiency = 4.78%, V_{oc} = 0.86 V). Whereas, under the same device fabrication conditions, **PaDTNBTH**- and **PaDTNBTF**-based devices exhibit efficiencies of 5.22% and 1.73%, respectively. Our results demonstrate that **aDTN** is a better building block in constructing p-type copolymers for high open circuit voltage devices compared to the linear-shaped **DTN**.

Received 23rd May 2014
Accepted 18th June 2014

DOI: 10.1039/c4ta02585g

www.rsc.org/MaterialsA

1. Introduction

Polymer solar cells (PSCs) have emerged as a promising alternative for producing green and renewable energy, because of their low-cost, light-weight, and great potential for fabrication as large-area flexible devices.[1–10] Efficient PSCs have been made using a bulk heterojunction (BHJ) structure, which comprises p-type polymers blended with n-type fullerene derivatives (such as $PC_{61}BM$ and $PC_{71}BM$). Recently, power conversion efficiencies (PCEs) of PSCs have reached up to 9.35% for single-junction devices and 10.6% for tandem cells, mainly thanks to the innovation in tailor-made photoactive materials as well as device processing technologies.[11,12] For the p-type materials, the most common and successful strategy currently is to design and synthesize D–A (electron donor–acceptor) copolymers,[8,13,14] owing to their small band gaps, deep-lying HOMO energy levels, and high hole mobilities.[15–18]

Planarization and rigidization of polyaromatic conjugated skeletons may facilitate a better π-electron delocalization, reduce the energetic disorder of the resulting polymers, and induce strong intermolecular interactions between the polymer chains for efficient charge transportation.[19] Moreover, an extended π-conjugated aromatic molecule with a multi-ring fused framework endows a broader, more intense absorption band, leading to an enhanced solar light harvesting.[20,21] Based on these guidelines, ladder-type structures, which are constructed by fastening or fusing adjacent aromatic units such as benzene or thiophene *via* a bridging atom, have attracted significant attention for photovoltaic applications. Besides their intrinsic properties, good solubility of these rigid rod-like polymers can be anticipated through the incorporation of various alkyl chains into the bridging atoms. Recently, a number of conjugated polymers based on ladder-type molecules have been reported by some research groups as well as by us.[19,20,22–37] For example, ladder-type indacenodithieno[3,2-*b*]-thiophene-based polymers were used to fabricate PSCs with PCEs up to 7.51%.[37] And PSCs with a V_{oc} as high as 1.06 V have been fabricated, based on ladder-type oligo-*p*-phenylene containing copolymers.[20] All these exciting achievements suggest

State Key Laboratory of Structural Chemistry, Fujian Institute of Research on the Structure of Matter, Chinese Academy of Sciences, Fuzhou, 350002, P. R. China. E-mail: qingdongzheng@fjirsm.ac.cn; Fax: +86-591-83721625

† Electronic supplementary information (ESI) available: Figures showing the absorption spectra of the blended films, the *J–V* characteristics for PSCs, external quantum efficiency curves of the devices, and summary of device parameters of PSCs. See DOI: 10.1039/c4ta02585g

that ladder-type molecules are an excellent class of building blocks for high performance copolymers in photovoltaic applications.

The isomeric phenomena generally originate from the position difference of the heteroatoms/functional groups or the bond connection styles of the molecular moieties.[38] They are very common in fused aromatic hydrocarbons. Recent studies indicate that the structural isomerization has a significant impact on the properties of organic electronic materials. For example, as shown in Fig. 1, picene has a better chemical stability and device performance than its isomer pentacene in air.[39] Takimiya *et al.* discovered that angular-shaped naphthodithiophenes (**NDTs**) showed deeper HOMO energy levels and larger band gaps than their linear counterparts. Interestingly, in comparison with their linear counterparts, angular-shaped **NDT**-based copolymer **PNDT3BT** could lead to a more ordered molecular packing, which facilitates an efficient carrier transport.[40,41] Similar results were also found by Müllen *et al.* regarding the investigation on the influence of backbone curvature on charge-carrier mobilities.[42,43] Recently, we reported a series of D–A copolymers based on ladder-type dithienonaphthalene (**DTN**) units. PSCs based on one of these **DTN**-containing copolymers (**PDTNTBT** in Fig. 1) exhibited a PCE of 4.78% with an open circuit voltage (V_{oc}) of 0.86 V, indicating that **DTN** is a promising donor unit for constructing high performance conjugated copolymers.[19] Similar to other fused aromatics, **DTN** also contains different isomers, such as linear- and angular-shaped analogues (**aDTN**) (Fig. 1). Considering the abovementioned dependence of material electronic properties on its chemical structure, we expect that **aDTN**-based polymers may exhibit different properties in comparison with their linear-shaped analogues.

Herein, we design and synthesize **aDTN** as a donor unit for constructing D–A conjugated copolymers. Similar to our previous studies,[19] benzo[*c*][1,2,5]thiadiazole (**BT**) is chosen as an acceptor unit because of its strong electron-accepting ability.[44,45] At the same time, two thiophene groups are flanked on both sides of the **BT** group to reduce the steric hindrance, if any, between the donor and the acceptor units. In order to further modulate and optimize the performance of the **aDTN**-based copolymers, two electron-donating hexyloxy groups and two electron-withdrawing fluorine atoms are introduced onto the **BT** heterocycle, generating 5,6-bis(hexyloxy)benzo[*c*][1,2,5]-thiadiazole (**BTO**) and 5,6-difluorobenzo[*c*][1,2,5]thiadiazole (**BTF**). Using these three monomers, three D–A copolymers (**PaDTNBTH**, **PaDTNBTO**, and **PaDTNBTF** in Scheme 2) are synthesized. The optical, electrochemical, and electrical properties, as well as the preliminary photovoltaic performance of these copolymers, are investigated. The results reveal that these copolymers possess deep-lying HOMO energy levels below −5.34 eV, with medium band gaps in the range of 1.79–1.90 eV. **PDTNTBT** differs from **PaDTNBTO** in the chemical structure of the donor unit for D–A copolymers. **DTN** is used for the former, whereas **aDTN** is used for the latter. However, the **PaDTNBTO**-based device exhibits a PCE of 6.44% with a V_{oc} of 0.92 V, which is higher than that of the **PDTNTBT**-based device (efficiency of 4.78% with a V_{oc} of 0.86 V).

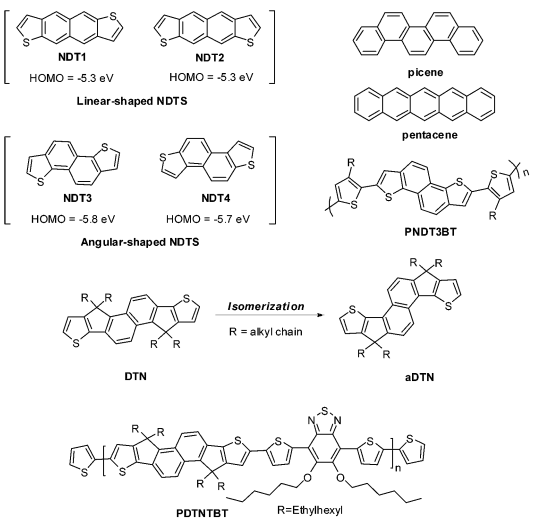

Fig. 1 Chemical structures of naphthodithiophene derivatives, NDT1-4, picene, pentacene, linear-shaped DTN, angular-shaped DTN, and PDTNTBT.

2. Experimental

2.1. Material

Reagents were purchased from Aldrich Inc., Aladdin-Reagent Inc. or Adamas-beta Ltd. and used without further purification unless otherwise specified. Compounds **1**, **9**, **10**, and **11** were prepared according to the literature procedures.[46–49] Column chromatography was conducted with silica gel (200–300 mesh).

2.2. Instruments

^{1}H and ^{13}C NMR spectra were collected on a Bruker AVANCE-400 spectrometer operating at 400 and 100 MHz in $CDCl_3$ or DMSO-d_6 with the TMS reference. High-resolution mass spectroscopy (HRMS) measurements were performed on an IonSpec 4.7T spectrometer. Gel permeation chromatography (GPC) was conducted in THF on a Waters 1515 system. The absorption spectra of the copolymers in chlorobenzene (1×10^{-5} M) and in thin films on glass substrates were measured by a Lambda 35 UV/vis spectrophotometer. Cyclic voltammetry (CV) was performed on a CHI 700E electrochemical workstation with a three-electrode system in a solution of 0.1 M Bu_4NPF_6 in acetonitrile at a scan rate of 100 mV s^{-1}. The copolymer films were coated on a Pt plate electrode by dipping the electrode into the corresponding solutions and then drying. A Pt wire was used as the counter electrode, and $Ag/AgNO_3$ was used as the reference electrode. Atomic force microscopy (AFM) was performed by a Veeco Multimode NS3A-02 Nanoscope III atomic force microscope. Blended films for AFM were prepared on PEDOT:PSS-coated ITO substrates prepared in identical fashion to those prepared for the device fabrication.

2.3. Fabrication of conventional PSCs

PSCs were fabricated in the traditional sandwich structure by using PEDOT:PSS (Baytron PVPAI 4083) as the anode buffer

layer. Indium tin oxide (ITO) glass was sequentially cleaned by ultrasonication in detergent, water, acetone, and isopropyl alcohol for 30 min each and then dried in an oven at 130 °C overnight. The ITO/glass substrates were first treated with oxygen plasma for 5 min, then PEDOT:PSS was spin-coated on the substrates at 3000 rpm for 1 min, and later the substrates were dried at 130 °C in air for 30 min. The active layer was prepared by spin-coating the polymer:$PC_{71}BM$ blends at 1000 rpm for 1 min in a glove box, and the devices were kept at room temperature for 12 h. Before the aluminum deposition, a conjugated polyelectrolyte **PIFB** was introduced as an interlayer to facilitate efficient electron injection. **PIFB** was prepared according to our previous report.[19] The **PIFB** layer (~1 nm) was obtained by spin-coating a methanol solution (0.3 mg mL^{-1} containing 30 eq. of acetic acid) on the top of the active layer. Ultimately, about 80 nm of aluminum was deposited on the top of the **PIFB** layer through shadow masks by thermal evaporation. The active area of the devices was fixed at 6 mm^2. All polymer:$PC_{71}BM$ blends were dissolved in mixed solvents of chlorobenzene and dichlorobenzene (4/1, v/v) at the concentration of 20 mg mL^{-1}. The blend ratio was fixed at 1 : 4 (polymer–$PC_{71}BM$ by weight).

2.4. Measurement of PSC devices

Device characterization was performed under AM 1.5G irradiation (100 mW cm^{-2}) on an Oriel sol3A simulator (Newport) with a NREL-certified silicon reference cell. The current density–voltage curves were measured by a Keithley 2440 source measurement unit.

2.5. Mobility measurements

Hole-only devices (ITO/PEDOT:PSS/polymer:$PC_{71}BM$/Au) and electron-only devices (ITO/Al/polymer:$PC_{71}BM$/Ca/Al) were fabricated in order to estimate the hole and electron mobilities of these polymers by the SCLC method. The hole-only devices were prepared following the same procedures used in photovoltaic device fabrication, except that the PIFB/Al cathode was replaced by the Au (40 nm) electrode. For the electron-only devices, Al (5 nm) was thermally evaporated on the pre-cleaned ITO; further, the BHJ film was coated using the same method as that used for the solar cell fabrication. Finally, Ca (20 nm) and Al (100 nm) were deposited on the BHJ film. The current density (J) was measured by an Agilent 4155C semiconductor parameter analyzer. The SCLC carrier mobilities were calculated according to the following equation:

$$J = \frac{9}{8}\varepsilon_r\varepsilon_0\mu\frac{V^2}{L^3} \quad (1)$$

where ε_0 is the permittivity of free space (8.85×10^{-12} F m^{-1}), ε_r is the dielectric constant of the polymer (assumed to be 3, which is a typical value for conjugated polymers), μ is the carrier mobility, V is the voltage drop across the device ($V = V_{appl} - V_r - V_{bi}$, where V_{appl} is the applied voltage to the device, V_r is the voltage drop due to the contact resistance and series resistance across the electrodes, and V_{bi} is the built-in voltage due to the difference in work function of the two electrodes), and L is the polymer thickness. The thickness of the film was measured by the Bruker Dektak XT surface profilometer.

2.6. Synthesis

1,5-Dibromo-2,6-bis(dibromomethyl)naphthalene.[50] A suspension of 1,5-dibromo-2,6-dimethylnaphthalene (**1**) (2.00 g, 6.4 mmol), *N*-bromosuccinimide (7.00 g, 39.3 mmol), dibenzoyl peroxide (0.95 g, 3.93 mmol) in anhydrous CCl_4 (75 mL) was refluxed for 24 h. After the removal of the solvent, the residue was filtered and washed with methanol and ethyl acetate, respectively. 1,5-Dibromo-2,6-bis(dibromomethyl)naphthalene (3.60 g, 90%) was obtained as a light yellow powder. ^{1}H NMR ($CDCl_3$, 400 MHz, ppm): 8.42 (d, J = 9.2 Hz, 2H), 8.21 (d, J = 9.2 Hz, 2H), 7.41 (s, 2H).

1,5-Bibromonaphthalene-2,6-dicarbaldehyde.[50] To a solution of 1,5-dibromo-2,6-bis(dibromomethyl)naphthalene (10.00 g, 15.82 mmol) in 640 mL of ethanol was added 160 mL of an aqueous $AgNO_3$ solution (10.76 g, 63.28 mmol) and the resulting solution was heated to reflux. After 2 h, a green precipitate was filtered by suction from the hot solution. A yellow solid appeared upon the removal of the solvent under reduced pressure. The solid was washed with ethanol–water (4 : 1 by volume) to obtain 1,5-dibromonaphthalene-2,6-dicarbaldehyde (5.23 g, 96%). ^{1}H NMR ($CDCl_3$, 400 MHz, ppm): 8.60 (d, J = 8.8 Hz, 2H), 8.11 (d, J = 8.8 Hz, 2H), 10.69 (s, 2H).

1,5-Dibromonaphthalene-2,6-dicarboxylic acid (2). To a solution of 1,5-dibromonaphthalene-2,6-dicarbaldehyde (3.80 g, 11.1 mmol) in 120 mL of *tert*-butanol was added 20 mL of 2-methyl-2-butene. An aqueous solution of $NaClO_2$ (20.10 g, 222 mmol) and $NaH_2PO_4 \cdot 2H_2O$ (24.20 g, 155 mmol) in 160 mL of water was added dropwise over 30 min. The resulting mixture was stirred for 24 h at room temperature. *tert*-Butanol was removed by rotary evaporation, and the resulting mixture was treated with 30 mL of H_2O and washed with 30 mL of hexane. A white solid was precipitated when the aqueous layer was acidified to pH 1. The precipitate was collected by filtration and washed with cold water to give 1,5-dibromonaphthalene-2,6-dicarboxylic acid as a white solid (3.60 g, 85%). ^{1}H NMR (DMSO-d_6, 400 MHz, ppm): 13.92 (s, 2H), 8.45 (d, J = 8.4 Hz, 2H), 7.91 (d, J = 8.4 Hz, 2H). ^{13}C NMR (DMSO-d_6, 100 MHz, ppm): 169.28, 137.75, 134.11, 129.42, 127.95, 126.36. HRMS (EI) *m*/*z*: calcd for $C_{12}H_6Br_2O_4$: 371.8633; found: 371.8630.

Dimethyl 1,5-dibromonaphthalene-2,6-dicarboxylate (3). Thionyl chloride (24.00 g, 202 mmol) was added dropwise to a solution of compound **2** (3.80 g, 10.1 mmol) in methanol (120 mL) at 0 °C. Then the resulting mixture was refluxed for 12 h, before cooling to 0 °C. The precipitate was collected by filtration and washed with cold methanol to give compound **3** (3.87, 94%) as a white solid. ^{1}H NMR ($CDCl_3$, 400 MHz, ppm): 8.51 (d, J = 8.8 Hz, 2H), 7.81 (d, J = 8.8 Hz, 2H), 4.03 (s, 6H). HRMS (EI) *m*/*z*: calcd for $C_{14}H_{10}Br_2O_4$: 399.8946; found: 399.8944.

Dimethyl 1,5-di(thiophen-2-yl)naphthalene-2,6-dicarboxylate (4). To a suspension of compound **3** (3.85 g, 9.58 mmol) in 96 mL of *N*,*N*-dimethylformamide (DMF) was added tributyl(thiophen-2-yl)stannane (7.86 g, 21.1 mmol). The mixture was

vigorously stirred and bubbled with N_2 for 1 h. Then 51 mg of $Pd(PPh_3)_2Cl_2$ was added to this degassed solution. The mixture was then heated at 85 °C under N_2 for 24 h. After being cooled to room temperature, the reaction mixture was poured into water and extracted with CH_2Cl_2 (3 × 50 mL). The organic layer was combined, then washed with water and brine, and then dried over anhydrous $MgSO_4$. After filtration, the filtrate was concentrated under reduced pressure. The residue was washed with methanol to afford compound **4** as a white solid (3.50 g, 90%). ^{1}H NMR ($CDCl_3$, 400 MHz, ppm): 7.97 (d, J = 8.8 Hz, 2H), 7.84 (d, J = 8.8 Hz, 2H), 7.55 (dd, J_1 = 1.2 Hz, J_2 = 5.2 Hz, 2H), 7.22 (dd, J_1 = 3.6 Hz, J_2 = 5.2 Hz 2H), 7.11 (dd, J_1 = 1.2 Hz, J_2 = 5.2 Hz, 2H), 3.72 (s, 6H). HRMS (MALDI) *m*/*z*: calcd for $C_{22}H_{16}O_4S_2$: 408.0490; found: 408.0485.

1,5-Di(thiophen-2-yl)naphthalene-2,6-dicarboxylic acid (5). To a solution of compound **4** (3.45 g, 8.46 mmol) in ethanol (120 mL), an aqueous solution of NaOH (4.74 g NaOH in 30 mL of H_2O) was added. The resulting mixture was heated at reflux overnight. After being cooled to room temperature, the solvent was removed under reduced pressure. Then, the residue was added to a concentrated hydrochloric acid solution. The precipitate was collected by filtration and washed with water then dried *in vacuo* to afford a white solid (3.10 g, 96%). ^{1}H NMR (DMSO-d_6, 400 MHz, ppm): 13.06 (s, 2H), 7.83 (q, J = 8.8 Hz, 4H), 7.78 (d, J = 5.2 Hz, 2H), 7.24 (dd, J_1 = 3.6 Hz, J_2 = 5.2 Hz 2H), 7.16 (d, J = 3.2 Hz, 2H). ^{13}C NMR (DMSO-d_6, 100 MHz, ppm): 169.30, 137.73, 134.15, 133.77, 131.17, 129.51, 127.90, 127.71, 127.67, 126.32. HRMS (MALDI) *m*/*z*: calcd for $C_{20}H_{12}O_4S_2$: 380.0177; found: 380.0172.

Compound 6. To a suspension of compound **5** (3.10 g, 8.16 mmol) in 100 mL of anhydrous CH_2Cl_2 was added 4.20 g of oxalyl chloride (32.64 mmol) and 0.3 mL of DMF. The resulting mixture was stirred overnight at room temperature. The solvent was removed to afford the intermediate dicarboxylic acid chloride as a yellow solid. Then the solid was dissolved in 20 mL of anhydrous CH_2Cl_2 again and then added to a suspension of $AlCl_3$ (6.50 g, 48.96 mmol) in 50 mL of CH_2Cl_2 at 0 °C. The resulting mixture was allowed to warm to room temperature with stirring overnight, and was then poured into ice-cold hydrochloride acid solution. The precipitate was collected by filtration and washed with water, then dried under vacuum to afford a deep blue solid (2.74 g, 98%). ^{1}H NMR ($CDCl_3$, 400 MHz, ppm): 7.84 (d, J = 8.0 Hz, 2H), 7.55 (d, J = 8.0 Hz, 2H), 7.26 (d, J = 8.0 Hz, 2H), 7.02 (d, J = 8.0 Hz, 2H). HRMS (MALDI) *m*/*z*: calcd for $C_{20}H_8O_2S_2$: 343.9966; found: 343.9960.

Compound 7. A mixture of compound **6** (2.80 g, 8.14 mmol), hydrazine monohydrate (8.14 g, 0.16 mol) and KOH (9.20 g, 0.16 mol) in 150 mL of diethylene glycol was heated at 180 °C for 24 h. Then the mixture was poured into ice-cold hydrochloride acid. The precipitate was collected by filtration and washed with water, then dried under vacuum to afford a pale yellow solid (2.50 g, 92%). ^{1}H NMR ($CDCl_3$, 400 MHz, ppm): 8.08 (d, J = 8.0 Hz, 2H), 7.77 (d, J = 8.0 Hz, 2H), 7.45 (d, J = 8.0 Hz, 2H), 7.24 (d, J = 8.0 Hz, 2H), 3.87 (s, 4H). HRMS (MALDI) *m*/*z*: calcd for $C_{20}H_{12}S_2$: 316.0380; found: 316.0375.

Compound aDTN. To a suspension of compound **7** (1.25 g, 4.0 mmol) in 40 mL of anhydrous DMSO was added sodium *tert*-butoxide (2.30 g, 24.0 mmol) in portions. The reaction mixture was heated at 80 °C for 1 h, followed by the dropwise addition of 2-ethylhexyl bromide (4.63 g, 24.0 mmol). After the addition, the resulting mixture was heated at 85–90 °C for 8 h, then poured into ice-water and extracted with CH_2Cl_2 (3 × 50 mL). The organic layer was dried over anhydrous $MgSO_4$ and the solvent was removed under reduced pressure to get the crude product. The crude product was purified by column chromatography on silica, eluting with petroleum ether, to give a yellow viscous oil (1.20 g, 40%). ^{1}H NMR ($CDCl_3$, 400 MHz, ppm): 8.01 (d, J = 8.0 Hz, 2H), 7.58 (d, J = 8.0 Hz, 2H), 7.37 (d, J = 8.0 Hz, 2H), 7.10 (d, J = 8.0 Hz, 2H), 2.00–2.07 (m, 8H), 1.26–0.48 (m, 60H). ^{13}C NMR ($CDCl_3$, 100 MHz, ppm): 157.22, 147.65, 141.15, 135.14, 129.73, 125.59, 124.12, 121.93, 118.15, 56.25, 44.48, 35.08, 33.45, 28.39, 26.59, 22.65, 14.03, 10.31. HRMS (MALDI) *m*/*z*: calcd for $C_{52}H_{76}S_2$: 764.5388; found: 764.5383.

Compound 8. *n*-Butyllithium (5.1 mL, 2.5 M in hexanes) was added dropwise to a solution of compound **aDTN** (2.45 g, 3.20 mmol) in 20 mL of THF at −78 °C. The mixture was stirred at −78 °C for 1 h. A solution of trimethyltin chloride (2.56 g in 10 mL of THF) was added dropwise. The reaction mixture was allowed to warm to room temperature and was stirred overnight. Then the mixture was poured into water and extracted with ether. The organic layer was washed with water and dried over $MgSO_4$. Evaporation of the solvent afforded compound **8** as a light brownish oil (3.10 g, 89%), which was not further purified but directly used in the next step. ^{1}H NMR ($CDCl_3$, 400 MHz, ppm): 8.07 (d, J = 8.0 Hz, 2H), 7.61 (d, J = 8.0 Hz, 2H), 7.07 (d, J = 8.0 Hz, 2H), 2.43–2.12 (m, 8H), 1.26–0.46 (m, 60H), 0.39 (s, 18H). ^{13}C NMR ($CDCl_3$, 100 MHz, ppm): 157.64, 150.50, 146.72, 139.72, 135.22, 129.95, 126.00, 122.08, 121.66, 53.51, 43.34, 34.86, 34.29, 28.42, 27.32, 22.81, 13.97, 10.42, −8.27. MS *m*/*z*: calcd for $C_{52}H_{76}S_2$ [M − $2Sn(CH_3)_3$] 764.5; found: 764.5.

PaDTNBTO. The monomer **8** (0.32 g, 0.29 mmol), 4,7-bis(5-bromothiophen-2-yl)-5,6-bis(hexyloxy)benzo[*c*][1,2,5]thiadiazole (**9**) (0.193 g, 0.29 mmol) in 20 mL of toluene, and 2 mL of DMF was degassed by bubbling with nitrogen for 1 h at room temperature. After the addition of 15 mg of $Pd(PPh_3)_4$, the mixture was heated to reflux for 3 days under an argon atmosphere. Then, 2-tributylstannylthiophene (54 mg, 0.15 mmol) was added to the mixture solution and reacted for 3 h. Finally, 2-bromothiophene (48 mg, 0.29 mmol) was added to the mixture and reacted overnight to complete the end-capping reaction. The mixture was cooled to room temperature and added dropwise into 200 mL of methanol. The solid was collected by filtration and extracted in a Soxhlet setup with methanol, acetone, and hexane for 24 h each. The insoluble remainders were redissolved in chloroform and reprecipitated into methanol. The target polymer was collected by filtration and dried *in vacuo* at 50 °C overnight to give a black solid (0.30 g, 89%) ^{1}H NMR ($CDCl_3$, 400 MHz, ppm): 8.62 (br, 2H), 8.08 (br, 2H), 7.66 (br, 2H), 7.46 (m, 2H), 7.39 (br, 2H), 4.27 (br, 4H), 2.10 (br, 8H), 1.47 (br, 8H), 1.05–0.59 (m, 64H). M_n = 54.5 kDa, polydispersity = 1.83. The low molecular weight polymer (**PaDTNBTO**) was synthesized using the same procedure but a shorter polymerization time (48 h). M_n = 10.3 kDa, polydispersity = 1.66.

PaDTNBTH. Polymer **PaDTNBTH** was prepared according to the same procedure as that for **PaDTNBTO**, using monomer **8** (0.32 g, 0.29 mmol) and compound **10** (0.134 g, 0.29 mmol). Yield: 0.23 g (79%). ^{1}H NMR ($CDCl_3$, 400 MHz, ppm): 8.16 (br, 2H), 8.07 (br, 2H), 7.95 (br, 2H), 7.67 (m, 2H), 7.43 (m, 2H), 7.40 (m, 2H), 2.12 (br, 8H), 1.05–0.59 (m, 60H). M_n = 25.5 kDa, polydispersity = 1.58.

PaDTNBTF. Polymer **PaDTNBTF** was prepared according to the same procedure as that for **PaDTNBTO**, using monomer **8** (0.32 g, 0.29 mmol) and compound **11** (0.145 g, 0.29 mmol). Yield: 0.19 g (62%). ^{1}H NMR ($CDCl_3$, 400 MHz, ppm): 8.34 (br, 2H), 8.05 (br, 2H), 7.67 (br, 2H), 7.46 (br, 2H), 7.44 (br, 2H), 2.14 (br, 8H), 1.05–0.60 (m, 60H). M_n = 15.7 kDa, polydispersity = 1.64.

3. Results and discussion

3.1. Synthesis and characterization

The synthetic routes for the monomer (**8**) and the copolymers are depicted in Schemes 1 and 2. All compounds were synthesized similarly to the method previously reported by us except for the key intermediate 1,5-dibromonaphthalene-2,6-dicarboxylic (**2**). Compound **2** was obtained by using a simplified procedure, which started from 1,5-dibromo-2,6-dimethylnaphthalene through a three-step process successively involving benzylic radical dibromination to 1,5-dibromo-2,6-bis(dibromomethyl)naphthalene, hydrolysis into the corresponding 1,5-dibromonaphthalene-2,6-dicarbaldehyde, and then oxidation into the corresponding carboxylic acid, to give a 73% overall yield. Compound **3** was obtained by an esterification reaction under the catalytic action of $SOCl_2$ in a 94% yield. The Stille coupling reaction between compound **3** and tributyl(thiophen-2-yl)stannane gave compound **4** in a 90% yield. Compound **4** was hydrolyzed to compound **5**, which was subsequently converted into an acid chloride derivative by reacting with oxalyl chloride. Further, intramolecular Friedel–Crafts acylation of the acid chloride derivative afforded a ketone (**6**) in a 98% yield. Compound **7** was obtained after a Wolf–Kishner reduction of compound **6** in a 92% yield. The alkylation of compound **7** afforded **aDTN** with four 2-ethylhexyl groups.

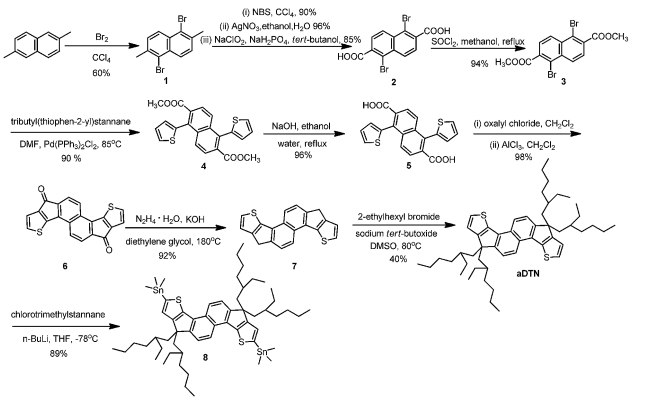

Scheme 1 Synthesis of the monomer.

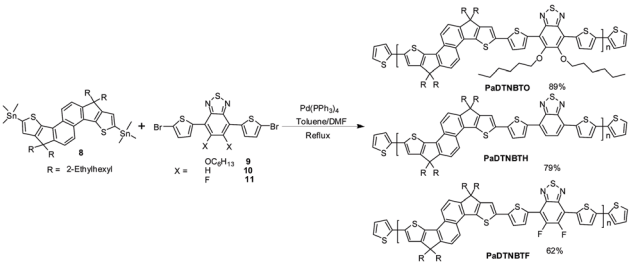

Scheme 2 The synthetic route for the aDTN-containing copolymers.

Compound **8** was synthesized in a 89% yield by the lithium–hydrogen exchange on **aDTN** and by reaction with trimethyltin chloride. Stille coupling reactions between monomer **8** and 4,7-bis(5-bromothiophen-2-yl)-5,6-bis(hexyloxy)benzo[*c*][1,2,5]thiadiazole (**9**), 4,7-bis(5-bromothiophen-2-yl)benzo[*c*][1,2,5]thiadiazole (**10**), and 4,7-bis(5-bromothiophen-2-yl)-5,6-difluorobenzo[*c*][1,2,5]thiadiazole (**11**) using palladium tetrakis(triphenylphosphine) ($Pd(PPh_3)_4$) as the catalyst gave the D–A copolymers **PaDTNBTO**, **PaDTNBTH**, and **PaDTNBTF** in 89%, 79% and 62% yields, respectively. These copolymers were purified by precipitation from methanol and subsequent Soxhlet extraction with methanol, acetone, hexane, and chloroform in sequence. Due to the four 2-ethylhexyl chains being introduced into both sides of the **aDTN** unit, all copolymers show good solubility in chlorinated solvents such as chloroform, chlorobenzene, and dichlorobenzene at room temperature. The number-average molecular weights (M_n) of **PaDTNBTO**, **PaDTNBTH**, and **PaDTNBTF**, are 54.5 kg, 25.5 kg, and 15.7 kg, respectively, with relatively narrow polydispersity indices (PDIs) in the range of 1.58–1.83 (Table 1), which were estimated by gel permeation chromatography (GPC) using THF as the eluent and polystyrene as the internal standard.

3.2. Optical properties

UV-vis absorption spectra of the copolymers in chlorobenzene solutions (1×10^{-5} M) and in thin films are shown in Fig. 2 and the optical parameters are summarized in Table 1. All the three copolymers exhibit one main broad absorption band in both dilute solutions and thin films. As shown in Fig. 2a, incorporating different substituents onto the **BT** unit have significant effects on the optical properties of the copolymers. For example, the absorption maximum of **PaDTNBTH** in chlorobenzene is located at 591 nm. After introducing two electron-donating hexyloxy groups, the absorption maximum of **PaDTNBTO** blue-shifts about 26 nm (λ_{max} = 565 nm). Interestingly, by adding two F atoms onto the **BT** unit, **PaDTNBTF** also shows a blue shift of about 5 nm compared to the nonfluorinated copolymer **PaDTNBTH**, indicating that the fluorine substitution on the **BT** unit has a certain influence on the optical properties of the resulting D–A copolymers. Similar results have also been found in some other fluorinated copolymer systems.[12,51–54] In going from solution to a solid film (Fig. 2b), negligible changes were observed in the absorption profiles, except that there are 10–32 nm red-shifted absorption peaks for the films. The optical

Table 1 Summary of the molecular weights and optical and electrochemical properties of the copolymers

Polymer	M_n (kg mol^{-1})	PDI	λ_{max} (nm) in chlorobenzene	λ_{max} (nm) in film	$E_g^{opt a}$ (eV)	HOMO^b (eV)	LUMO^c (eV)	E_g^{ecd} (eV)
PaDTNBTO	54.5	1.83	565	575	1.90	−5.40	−3.57	1.83
PaDTNBTH	25.5	1.58	591	623	1.79	−5.34	−3.58	1.76
PaDTNBTF	15.7	1.64	586	617	1.81	−5.38	−3.59	1.79

[a] Estimated from the onset of the absorption spectra of thin films. [b] $E_{HOMO} = -(\varphi_{ox} + 4.82)$ eV. [c] $E_{LUMO} = -(\varphi_{red} + 4.82)$ eV. [d] E_g^{ec} = electrochemical band gap (LUMO–HOMO).

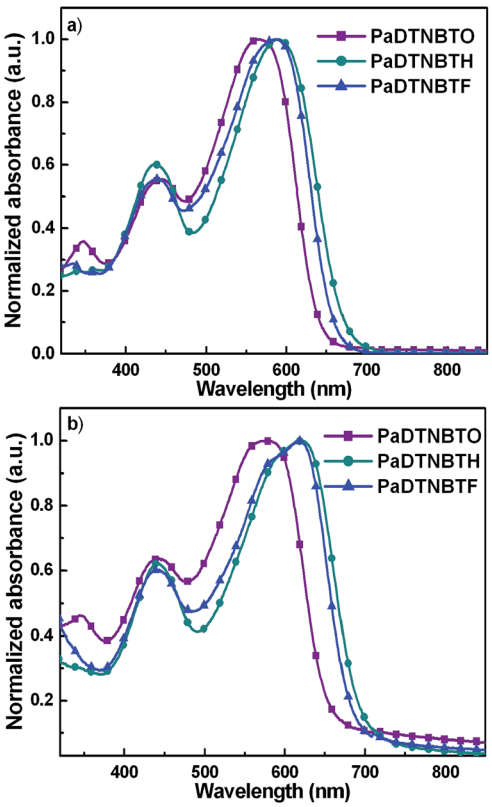

Fig. 2 Absorption spectra of the target copolymers in chlorobenzene (a) and in solid film (b).

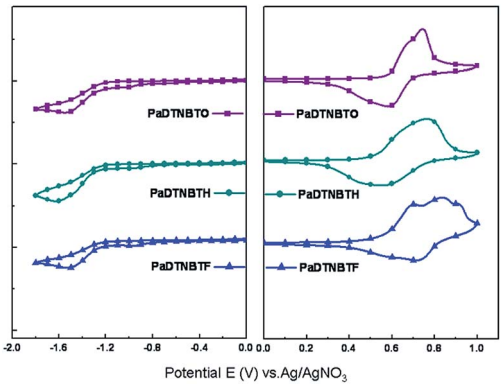

Fig. 3 Cyclic voltammogram (CV) of the copolymer films on a platinum electrode at a scan rate of 100 mV s^{-1}.

bandgaps (E_g^{opt}) deduced from the absorption edges (λ_{edge}) of the polymer films are 1.90, 1.79, and 1.81 eV for **PaDTNBTO**, **PaDTNBTH**, and **PaDTNBTF**, respectively.

3.3. Electrochemical properties

The molecular frontier orbitals of the target copolymers were investigated by the cyclic voltammetry (CV) method in films on a Pt disk working electrode in 0.1 M Bu_4NPF_6 acetonitrile solutions at a scan rate of 100 mV s^{-1}. Under this condition, the onset oxidation potential ($E_{1/2ox}$) of ferrocene was −0.02 V *versus* Ag/Ag$^+$. The CV curves were calibrated using ferrocene as the standard, whose HOMO energy level was set at −4.80 eV. Fig. 3 shows the cyclic voltammetry for these copolymers. From the onset oxidation (φ_{ox}) and the reduction potentials (φ_{red}) *versus* Ag/Ag$^+$ in the cyclic voltammogram, the HOMO and LUMO energy levels, as well as the band gaps (E_g^{ec}) of the copolymers, were estimated according to the following equations, with the detailed data summarized in Table 1.

$$E_{HOMO} = -(\varphi_{ox} + 4.82)(eV) \quad (2)$$

$$E_{LUMO} = -(\varphi_{red} + 4.82)(eV) \quad (3)$$

$$E_g^{ec} = (\varphi_{ox} - \varphi_{red})(eV) \quad (4)$$

As shown in Fig. 3, all the three copolymers exhibit reversible anodic oxidation and irreversible cathodic reduction curves in cyclic voltammetry measurements. For **PaDTNBTH**, the φ_{ox} and the φ_{red} are 0.52 V and −1.24 V, respectively, corresponding to a HOMO level of −5.34 eV and a LUMO level of −3.58 eV. After adding two F atoms, **PaDTNBTF** exhibits a relatively deeper HOMO level of −5.38 eV, whereas the LUMO level (−3.59 eV) is almost unchanged. Similar trends in the HOMO level change have also been found in some other fluorinated copolymer systems.[55,56] Interestingly, when the F atom was exchanged to the hexyloxy group, **PaDTNBTO** shows a deeper HOMO level of −5.40 eV and an equivalent LUMO level of −3.57 eV compared to that of **PaDTNBTF**, which could be attributed to the decreased charge transfer from the donor moiety to the acceptor moiety (BT) with the incorporation of two electron-donating hexyloxy groups. Clearly, the HOMO energy levels of all copolymers are low enough to ensure good stability and a high V_{oc} in PSCs. As we know, V_{oc} is positively correlated with the offset between the HOMO energy levels of donor materials and the LUMO energy levels of acceptor materials.[57] Meanwhile, the

LUMO level difference between the polymers and $PC_{71}BM$ (−4.3 eV) are ~0.7 eV, which means that electron transfer from the polymers to $PC_{71}BM$ is energetically favorable. The band gaps calculated from the difference between the onset oxidation and reduction potentials are 1.83, 1.76, and 1.79 eV for **PaDTNBTO**, **PaDTNBTH**, and **PaDTNBTF**, in that order. The results are in agreement with its optical band gaps, within experimental error.

3.4. Hole mobilities and photovoltaic properties

The hole mobilities of the copolymers were investigated by using the space-charge limited current (SCLC) method with a device structure of ITO/PEDOT:PSS (40 nm)/polymer:$PC_{71}BM$/Au (40 nm). The linear fits for the plots of $J^{0.5}$ *versus* V ($V = V_{appl} - V_r - V_{bi}$, where V_{appl} is the applied voltage to the device, V_r is the voltage drop due to contact resistance and series resistance across the electrodes, and V_{bi} is the built-in voltage due to the difference in work function of the two electrodes) are shown in Fig. 4 and the data are collected in Table S1.† The hole mobilities are estimated to be 2.81×10^{-5}, 3.69×10^{-5}, and 7.5×10^{-6} $cm^2 V^{-1} s^{-1}$ for the blends of **PaDTNBTO**, **PaDTNBTH**, and **PaDTNBTF** with $PC_{71}BM$, respectively. Obviously, as donor materials, **PaDTNBTO** and **PaDTNBTH** will have some advantages in the photovoltaic application compared to **PaDTNBTF**, due to their higher hole mobilities.

The photovoltaic properties of the resulting copolymers were investigated with a conventional device structure of ITO/PEDOT:PSS (40 nm)/polymer:$PC_{71}BM$/PIFB/Al (80 nm). Here, a thin layer of **PIFB** was employed as the cathode interlayer.[19] $PC_{71}BM$ was chosen as the electron acceptor due to its broader and stronger absorption in the visible region, which is complementary to the absorption valley of the polymer and beneficial for high efficient PSCs.[58] The active layers were prepared by spin coating the polymer:$PC_{71}BM$ blends from mixed solvents (chorobenzene–*o*-dichorobenzene = 4 : 1, v/v) on the top of the PEDOT:PSS layer without any further treatment. The measurements were performed under simulated AM1.5G, 100 mW cm^{-2} illumination with an active area of 0.06 cm^2. The current density–voltage (*J*–*V*) characteristics of these PSCs are shown in Fig. 5 and 7, and the device parameters such as V_{oc}, short-circuit current density (J_{sc}), fill factor (FF), and PCE are summarized in Table 2.

The donor–acceptor (D–A) ratio plays an important role in the performance of PSCs, because a balance in the hole and electron transport is necessary to avoid any accumulation of charge and thus to facilitate the charge transport process during the photon-to-current conversion.[37,59] Therefore, we fabricated PSC devices based on **PaDTNBTO**:$PC_{71}BM$ with different blend ratios to optimize the device performance. Fig. 5 shows the *J*–*V* curves and the external quantum efficiency (EQE) spectra of the devices with different blend ratios (D–A = 1 : 2, 1 : 3, 1 : 4, 1 : 5), with the detailed parameters summarized in Table 2. In Table 2, the device parameters of the **PDTNTBT**-based solar cell are listed as a reference.[19] It should be mentioned that the only difference in **PaDTNBTO** and **PDTNTBT** is the donor unit (Fig. 1 and Scheme 2). However, the device based on **PaDTNBTO** (blend ratio of 1 : 4) gives the best PCE of 6.44% with a V_{oc} of 0.92 V, a J_{sc} of 10.91 mA cm^{-2} and an FF of 64.1%, which is higher than the best PCE of 4.78% with a V_{oc} of 0.86 V, a J_{sc} of 10.29 mA cm^{-2} and an FF of 53.8% for the **PDTNTBT**-based device. The EQE spectra (Fig. 5b) show that the device with the 1 : 4 blend ratio has higher EQE values in the range from 360 to 610 nm, compared to those of the devices with other blend ratios. In order to reveal the impact of D–A ratio on the photovoltaic parameters, the V_{oc}, J_{sc}, FF and PCE data are plotted in Fig. 6a–d as functions of the blend ratio. It can be seen that the

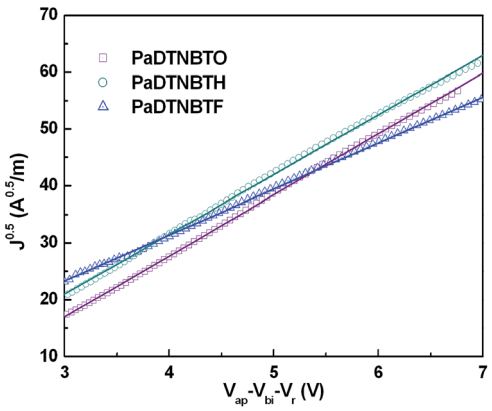

Fig. 4 $J^{0.5}$–*V* characteristics of hole-only devices based on different polymers.

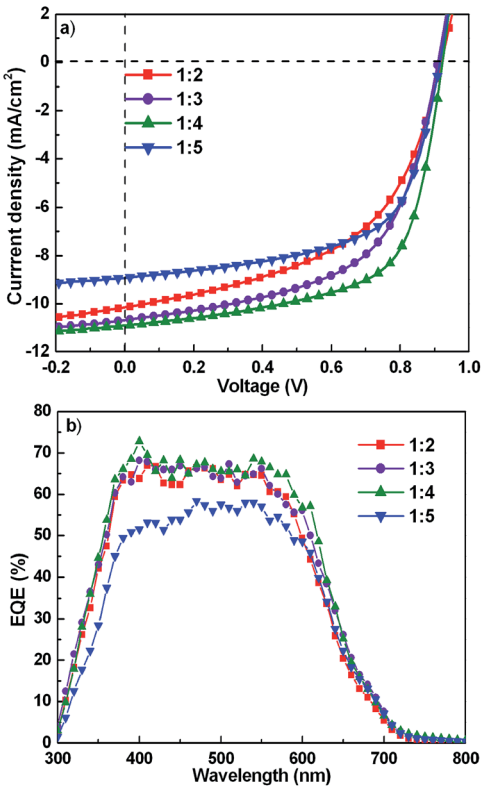

Fig. 5 (a) Current density (*J*)–voltage (*V*) characteristics, and (b) EQE curves of BHJ solar cells based on **PaDTNBTO** with various blend ratios.

Table 2 Device parameters of PSCs based on three copolymers

Polymers	D–A ratio (w/w)	V_{oc} (V)	J_{sc} (mA cm^{-2})	FF (%)	PCE$_{ave}$[a] (%)	PCE$_{max}$ (%)	Ref.
PaDTNBTO	1 : 2	0.92	9.98 ± 0.15	51.2 ± 0.4	4.66 ± 0.14	4.80	This work
	1 : 3	0.91	10.62 ± 0.04	56.7 ± 0.8	5.47 ± 0.13	5.60	This work
	1 : 4	0.92	10.62 ± 0.29	63.9 ± 0.2	6.29 ± 0.15	6.44	This work
	1 : 5	0.91	8.28 ± 0.62	61.2 ± 0.4	4.62 ± 0.39	5.01	This work
	1 : 4[b]	0.89	10.55 ± 0.24	52.0 ± 0.7	4.81 ± 0.22	5.03	This work
PaDTNBTH	1 : 4	0.90	11.12 ± 0.05	51.3 ± 0.5	5.13 ± 0.09	5.22	This work
PaDTNBTF	1 : 4	0.91	3.95 ± 0.04	47.2 ± 0.6	1.70 ± 0.03	1.73	This work
PDTNTBT	1 : 3	0.86	10.29	53.8	—	4.78	19

[a] The average PCE is obtained from eight devices. [b] PSC devices based on low molecular weight **PaDTNBTO** (M_n = 10.3 kg mol^{-1}; PDI = 1.7).

blend ratio significantly affects the J_{sc} and FF, although the V_{oc} is nearly unchanged regardless of the blend ratio. For example, when the blend ratio increases from 1 : 2 to 1 : 4, the J_{sc} of the devices gradually increases from 10.13 to 10.93 mA cm^{-2}, and the FF of the device increases from 51.6% to 64.1%, while a high V_{oc} of 0.92 V is retained. This effect is probably due to the more balanced hole and electron mobilities in the blend films with high $PC_{71}BM$ contents, which prevents the accumulation of charges. Moreover, the active layer of high $PC_{71}BM$ content devices may have a bicontinuous phase separation with the appropriate domain size, which affords efficient exciton diffusion and charge separation. When the blend ratio further increases from 1 : 4 to 1 : 5, both the J_{sc} and FF of the devices decrease, leading to a reduced PCE of 5.01%. Therefore, the blend ratio of 1 : 4 was chosen as the optimal blend ratio for the other polymer blends.

In order to verify the above hypothesis, the morphology of the polymer blends with different blend ratios (D–A = 1 : 2, 1 : 3, 1 : 4, and 1 : 5) were investigated using tapping mode AFM. According to the topography images of the blend films, as shown in Fig. S4,† the root-mean-square (RMS) values of the **PaDTNBTO**:$PC_{71}BM$ blends at weight ratios of 1 : 2, 1 : 3, 1 : 4, and 1 : 5 are 0.52, 1.37, 1.87, and 2.15 nm, respectively. The larger RMS value in the blend films with higher $PC_{71}BM$ contents is probably attributed to the higher degree of $PC_{71}BM$ aggregation. For low $PC_{71}BM$ content film (D–A = 1 : 2, Fig. S4b†), $PC_{71}BM$ is dispersed into the polymer phase, and thus, the blend film did not form phase separation with an ideal domain size. In the case of the 1 : 5 blend ratio (Fig. S4h†), the phase separation is not optimal because of the over-dominant $PC_{71}BM$ in the polymer blend. For the blend films with D–A = 1 : 3 (Fig. S4d†) and 1 : 4 (Fig. S4f†) ratios, the films exhibit phase separation with an optimal domain size of 10–20 nm, which is favorable for efficient exciton dissociation and charge transport. Moreover, we measured the electron and hole mobilities by using the SCLC method to investigate the charge transport properties of the blend films with different blend ratios. Fig. S3† shows the dark current density–voltage (J_{dark}–V) characteristics of the hole-only devices and the electron-only devices with different blend ratios, with the detailed results summarized in Table S2.† It could be found that the hole and the electron mobilities are simultaneously improved with an increase in the $PC_{71}BM$ content in the **PaDTNBTO**:$PC_{71}BM$ blend films (D–A ratio from 1 : 2 to 1 : 4). When the $PC_{71}BM$ content was further increased (D–A = 1 : 5), the electron mobility continues to increase but the hole mobility starts to decrease. Finally, the electron and hole mobilities of the blend are more balanced at the weight ratio of 1 : 4, and are 5.26 × 10^{-5} and 2.81 × 10^{-5} cm^2 V^{-1} s^{-1}, respectively. When the FF values of the PSC devices are correlated with the blend ratios, it can be concluded that D–A ratios in the blend film play an important role in realizing balanced hole and electron mobilities, which is the key to achieving a high FF.

Under the same blend ratio of 1 : 4, as shown in Fig. 7a, the PSC device based on **PaDTNBTF** exhibited a quite low PCE of 1.73% with V_{oc} = 0.91 V, J_{sc} = 3.99 mA cm^{-2}, and FF = 47.8%. However, dramatically improved photovoltaic performance was achieved for the device based on **PaDTNBTH**, which exhibited a V_{oc} of 0.90 V, a slightly increased FF of 51.8%, and a significantly improved J_{sc} of 11.17 mA cm^{-2}, resulting in a moderate PCE of 5.22%. The best photovoltaic performance was obtained for the device based on **PaDTNBTO**, which showed a further improved FF of 64.1%, V_{oc} of 0.92 V, and a slightly decreased J_{sc} of 10.91 mA cm^{-2}, leading to a high PCE of 6.44%. It should be noted that such a promising performance was achieved without the use of any pre- and/or post-treatments, such as thermal

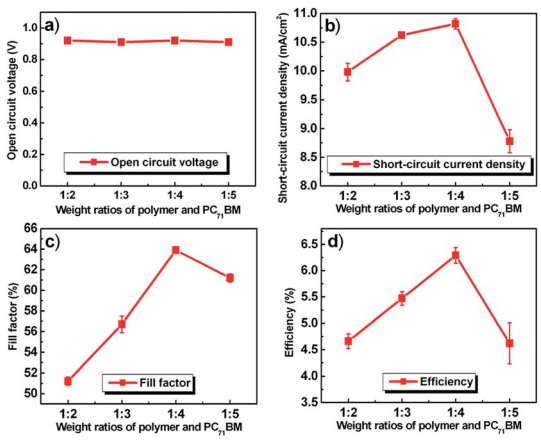

Fig. 6 The photovoltaic parameters of the PSCs based on PaDTNBTO:$PC_{71}BM$ with different blend ratios.

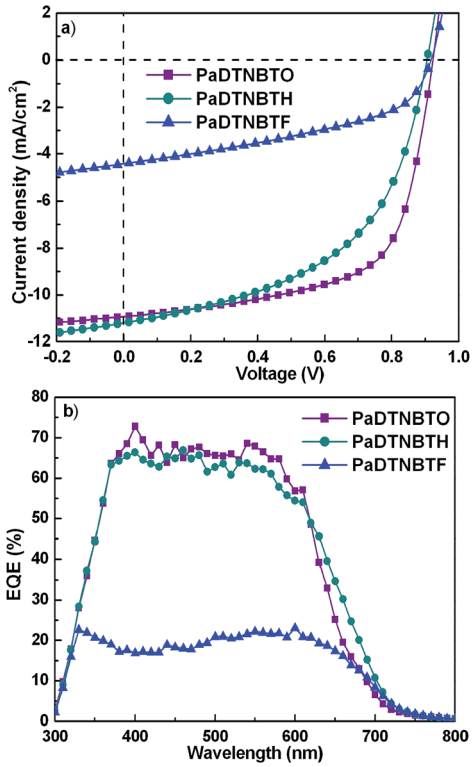

Fig. 7 (a) *J*–*V* characteristics and (b) EQE curves of BHJ solar cells based on the three copolymers.

annealing, solvent annealing, or processing additives. In our case, utilization of the different treatment methodologies only has negative effects on the device performance for the **PaDTNBTO**-based devices. The device parameters for all the devices fabricated in the different conditions are shown in Fig. S2 and Table S3.†

It was found that the J_{sc} and FF values of the **PaDTNBTH**- and **PaDTNBTO**-based devices are much higher than those based on **PaDTNBTF**, which could be ascribed to the optimal morphology with an appropriate domain size of the active layers based on **PaDTNBTH** and **PaDTNBTO**, as well as their higher charge carrier mobilities that promote charge transport in devices. As shown in Table 2, an increase in the molecular weight of **PaDTNBTO** leads to an improved device performance. When the M_n increases from 10.3 kg to 54.5 kg, maximum PCE increases from 5.03% to 6.44%, mainly due to the higher FF (64.1% *versus* 52.2%). These results have also been observed in previously reported literature.[60] Considering the fact that the molecular weight plays an important role in the device performance, we believe that there is still room to further improve the performance of the devices based on these copolymers through an optimization of their molecular weights. As we expected, devices based on **aDTN**-containing copolymers show a relatively higher V_{oc} in the range of 0.90–0.92 V compared to those based on linear-shaped **DTN**-containing copolymers (0.75–0.87 V),[19] which can be attributed to their deeper-lying HOMO energy levels.

3.5. External quantum efficiency

The external quantum efficiency (EQE) curves for the polymer-based devices under monochromatic light illumination are shown in Fig. 7b. As shown in the figure, the EQE curves for all the devices are rather flat in the wavelength range from 400 to 600 nm. The device based on **PaDTNBTO** exhibits a similar average EQE value to that based on **PaDTNBTH** (44.4% *versus* 44.7%) in the range of 300–750 nm, and both of them are much higher than that based on **PaDTNBTF** (16.5%). This result is consistent with the higher J_{sc} for the **PaDTNBTO**- or **PaDTNBTH**-based devices compared to that for the **PaDTNBTF**-based device. In addition, the photoresponse ranges for the devices based on **PaDTNBTH** and **PaDTNBTF** are slightly broader compared to that for the **PaDTNBTO**-based device, which is in agreement with the optical absorption spectra of the corresponding polymer:$PC_{71}BM$ blends in the same blend ratio (Fig. S1†).

3.6. Morphology

For polymer solar cells, the morphological control of the BHJ active layer is of great importance in charge generation, separation, and transport, which could influence final device performances. In this work, the surface morphological

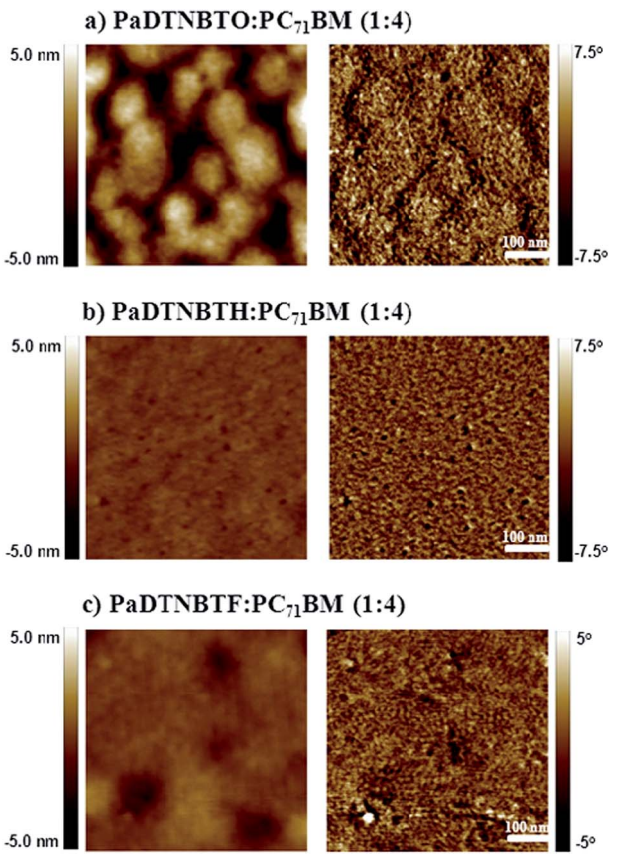

Fig. 8 Tapping mode AFM topography (left) and phase (right) images of blend films spin coated from polymer–$PC_{71}BM$ (1 : 4, w/w) (a) **PaDTNBTO**:$PC_{71}BM$, (b) **PaDTNBTH**:$PC_{71}BM$, (c) **PaDTNBTF**:$PC_{71}BM$ (all image sizes are 0.5 μm × 0.5 μm).

structures of the polymer–$PC_{71}BM$ (1 : 4, w/w) blend films were evaluated by using tapping mode AFM. The AFM topography and phase images are shown in Fig. 8. As can be seen in Fig. 8, phase separation was clearly observed for all the three polymer blends. Due to the structural differences in the three copolymers, the phase separation images for the blended films look different. For example, the film of the **PaDTNBTF**:$PC_{71}BM$ blend does not show uniform phase separation with many domain sizes over 40 nm, which is much larger than the typical exciton diffusion length of ~10 nm.[1,61] This can be accounted for by the low FF of 47.8% found in the **PaDTNBTF**-based device. The phase image of the film from **PaDTNBTH** blended with $PC_{71}BM$ displays a very smooth surface without any clear phase separation, which is also unfavorable for effective charge separation and transportation. In the case of the **PaDTNBTO**:$PC_{71}BM$ blend, a more clear phase separation could be observed with a domain size of ~20 nm. This is beneficial for the efficient exciton diffusion to the donor-acceptor interface, and thus contributes to the high FF of 64.1% for the **PaDTNBTO**-based device. The obtained root-mean-square roughness (RMS) values are 1.87, 0.72, and 0.25 nm for the blend films of **PaDTNBTO**:$PC_{71}BM$, **PaDTNBTF**:$PC_{71}BM$ and **PaDTNBTH**:$PC_{71}BM$, respectively. The difference in the RMS value can be attributed to the different substituents in the **BT** unit. Because the longer and bulkier side chains will create more disorder in the film self-organization, it is not surprising that the film based on the copolymers with two hexyloxy groups is the coarsest, and that based on the copolymers without any substitutes is the smoothest.

4. Conclusions

In summary, a novel ladder-type angular-shaped electron-rich unit (**aDTN**) has been designed and synthesized. Three D–A copolymers based on **aDTN** exhibit medium band-gaps in the range of 1.79–1.90 eV, along with deep-lying HOMO levels below −5.34 eV. As a result of the deep-lying HOMO level, BHJ photovoltaic devices derived from these polymers have a relatively high V_{oc} over 0.9 V. In particular, the photovoltaic device based on **PaDTNBTO** exhibits the best efficiency of 6.44%, which is higher than that of the device based on linear-shaped **DTN**-containing copolymers (**PDTNTBT**).[19] These preliminary results demonstrate that **aDTN** is a more promising electron-rich building block in constructing p-type copolymers for solar cells with high open circuit voltages compared to the linear-shaped **DTN**. Compared with other large band-gap materials such as P3HT, **PaDTNBTO** shows an improved performance in V_{oc}, which makes it a promising candidate for the short wavelength absorbing materials used for tandem PSCs.

Acknowledgements

This work was supported by the National Science Foundation of China (no. 51173186, 61325026), the National Basic Research 973 Program (no. 2011CB935904), the Key Project of Department of Science and Technology of Fujian Province (no. 2012H0044) and the 100 Talents Programme of the Chinese Academy of Sciences (CAS).

Notes and references

1 G. Yu, J. Gao, J. Hummelen, F. Wudl and A. J. Heeger, *Science*, 1995, **270**, 1789–1790.
2 J. Huang, Z. Yin and Q. Zheng, *Energy Environ. Sci.*, 2011, **4**, 3861–3877.
3 Y.-J. Cheng, S.-H. Yang and C.-S. Hsu, *Chem. Rev.*, 2009, **109**, 5868–5923.
4 Z. Yin and Q. Zheng, *Adv. Energy Mater.*, 2012, **2**, 179–218.
5 J. Chen and Y. Cao, *Acc. Chem. Res.*, 2009, **42**, 1709–1718.
6 O. InganÄs, F. Zhang and M. R. Andersson, *Acc. Chem. Res.*, 2009, **42**, 1731–1739.
7 Z. B. Henson, K. Müllen and G. C. Bazan, *Nat. Chem.*, 2012, **4**, 699–704.
8 G. Li, R. Zhu and Y. Yang, *Nat. Photonics*, 2012, **6**, 153–161.
9 Y. Li, *Acc. Chem. Res.*, 2012, **45**, 723–733; I. McCulloch, R. S. Ashraf, L. Biniek, H. Bronstein, C. Combe, J. E. Donaghey, D. I. James, C. B. Nielsen, B. C. Schroeder and W. Zhang, *Acc. Chem. Res.*, 2012, **45**, 714–722.
10 L. Ye, S. Zhang, L. Huo, M. Zhang and J. Hou, *Acc. Chem. Res.*, 2014, **47**, 1595–1603.
11 S.-H. Liao, H.-J. Jhuo, Y.-S. Cheng and S.-A. Chen, *Adv. Mater.*, 2013, **25**, 4766–4771.
12 J. You, L. Dou, K. Yoshimura, T. Kato, K. Ohya, T. Moriarty, K. Emery, C.-C. Chen, J. Gao, G. Li and Y. Yang, *Nat. Commun.*, 2013, **4**, 1446.
13 Z. He, C. Zhong, X. Huang, W.-Y. Wong, H. Wu, L. Chen, S. Su and Y. Cao, *Adv. Mater.*, 2011, **23**, 4636–4643.
14 L. Wang, D. Cai, Q. Zheng, C. Tang, S.-C. Chen and Z. Yin, *ACS Macro Lett.*, 2013, **2**, 605–608.
15 R. Qin, W. Li, C. Li, C. Du, C. Veit, H.-F. Schleiermacher, M. Andersson, Z. Bo, Z. Liu, O. Inganaäs, U. Wuerfel and F. Zhang, *J. Am. Chem. Soc.*, 2009, **131**, 14612–14613.
16 S. H. Park, A. Roy, S. Beaupré, S. Cho, N. Coates, J. S. Moon, D. Moses, M. Leclerc, K. Lee and A. J. Heeger, *Nat. Photonics*, 2009, **3**, 297–302.
17 C. E. Small, S. Chen, J. Subbiah, C. M. Amb, S.-W. Tsang, T.-H. Lai, J. R. Reynolds and F. So, *Nat. Photonics*, 2012, **6**, 115–120.
18 S. Albrecht, S. Janietz, W. Schindler, J. Frisch, J. Kurpiers, J. Kniepert, S. Inal, P. Pingel, K. Fostiropoulos, N. Koch and D. Neher, *J. Am. Chem. Soc.*, 2012, **134**, 14932–14944.
19 Y. Ma, Q. Zheng, Z. Yin, D. Cai, S.-C. Chen and C. Tang, *Macromolecules*, 2013, **46**, 4813–4821.
20 Q. Zheng, B. J. Jung, J. Sun and H. E. Katz, *J. Am. Chem. Soc.*, 2010, **132**, 5394–5404.
21 Y. Ma, Y. Sheng, C. Tang, X. Hong, S.-C. Chen, D. Zhu and Q. Zheng, *Sens. Actuators, B*, 2013, **176**, 132–140.
22 D. Cai, Q. Zheng, S.-C. Chen, Q. Zhang, C.-Z. Lu, Y. Sheng, D. Zhu, Z. Yin and C. Tang, *J. Mater. Chem.*, 2012, **22**, 16032–16040.
23 Q. Zheng, S. Chen, B. Zhang, L. Wang, C. Tang and H. E. Katz, *Org. Lett.*, 2010, **13**, 324–327.

24 B. C. Schroeder, Z. Huang, R. S. Ashraf, J. Smith, P. D'Angelo, S. E. Watkins, T. D. Anthopoulos, J. R. Durrant and I. McCulloch, *Adv. Funct. Mater.*, 2012, **22**, 1663–1670.
25 Z. Fei, R. S. Ashraf, Z. Huang, J. Smith, R. J. Kline, P. D'Angelo, T. D. Anthopoulos, J. R. Durrant, I. McCulloch and M. Heeney, *Chem. Commun.*, 2012, **48**, 2955–2957.
26 B. C. Schroeder, R. S. Ashraf, S. Thomas, A. J. P. White, L. Biniek, C. B. Nielsen, W. Zhang, Z. Huang, P. S. Tuladhar, S. E. Watkins, T. D. Anthopoulos, J. R. Durrant and I. McCulloch, *Chem. Commun.*, 2012, **48**, 7699–7701.
27 C.-P. Chen, S.-H. Chan, T.-C. Chao, C. Ting and B.-T. Ko, *J. Am. Chem. Soc.*, 2008, **130**, 12828–12833.
28 Y.-J. Cheng, J.-S. Wu, P.-I. Shih, C.-Y. Chang, P.-C. Jwo, W.-S. Kao and C.-S. Hsu, *Chem. Mater.*, 2011, **23**, 2361–2369.
29 Y.-J. Cheng, C.-H. Chen, Y.-S. Lin, C.-Y. Chang and C.-S. Hsu, *Chem. Mater.*, 2011, **23**, 5068–5075.
30 Y.-L. Chen, C.-Y. Chang, Y.-J. Cheng and C.-S. Hsu, *Chem. Mater.*, 2012, **24**, 3964–3971.
31 Y.-X. Xu, C.-C. Chueh, H.-L. Yip, F.-Z. Ding, Y.-X. Li, C.-Z. Li, X. Li, W.-C. Chen and A. K. Y. Jen, *Adv. Mater.*, 2012, **24**, 6356–6361.
32 J. J. Intemann, K. Yao, H.-L. Yip, Y.-X. Xu, Y.-X. Li, P.-W. Liang, F.-Z. Ding, X. Li and A. K. Y. Jen, *Chem. Mater.*, 2013, **25**, 3188–3195.
33 X. Xu, P. Cai, Y. Lu, N. S. Choon, J. Chen, B. S. Ong and X. Hu, *Macromol. Rapid Commun.*, 2013, **34**, 681–688.
34 H. Usta, C. Risko, Z. Wang, H. Huang, M. K. Deliomeroglu, A. Zhukhovitskiy, A. Facchetti and T. J. Marks, *J. Am. Chem. Soc.*, 2009, **131**, 5586–5608.
35 P. Sakthivel, H. S. Song, N. Chakravarthi, J. W. Lee, Y.-S. Gal, S. Hwang and S.-H. Jin, *Polymer*, 2013, **54**, 4883–4893.
36 J. Cao, Q. Liao, X. Du, J. Chen, Z. Xiao, Q. Zuo and L. Ding, *Energy Environ. Sci.*, 2013, **6**, 3224–3228.
37 X. Guo, M. Zhang, J. Tan, S. Zhang, L. Huo, W. Hu, Y. Li and J. Hou, *Adv. Mater.*, 2012, **24**, 6536–6541.
38 Z. Zhao, F. Zhang, X. Zhang, X. Yang, H. Li, X. Gao, C.-a. Di and D. Zhu, *Macromolecules*, 2013, **46**, 7705–7714.
39 H. Okamoto, N. Kawasaki, Y. Kaji, Y. Kubozono, A. Fujiwara and M. Yamaji, *J. Am. Chem. Soc.*, 2008, **130**, 10470–10471.
40 I. Osaka, T. Abe, S. Shinamura and K. Takimiya, *J. Am. Chem. Soc.*, 2011, **133**, 6852–6860.
41 S. Shinamura, I. Osaka, E. Miyazaki, A. Nakao, M. Yamagishi, J. Takeya and K. Takimiya, *J. Am. Chem. Soc.*, 2011, **133**, 5024–5035.
42 R. Rieger, D. Beckmann, A. Mavrinskiy, M. Kastler and K. Müllen, *Chem. Mater.*, 2010, **22**, 5314–5318.
43 R. Rieger, D. Beckmann, W. Pisula, W. Steffen, M. Kastler and K. Müllen, *Adv. Mater.*, 2010, **22**, 83–86.
44 D. Mühlbacher, M. Scharber, M. Morana, Z. Zhu, D. Waller, R. Gaudiana and C. Brabec, *Adv. Mater.*, 2006, **18**, 2884–2889.
45 J. Peet, J. Y. Kim, N. E. Coates, W. L. Ma, D. Moses, A. J. Heeger and G. C. Bazan, *Nat. Mater.*, 2007, **6**, 497–500.
46 S. Zeng, L. Yin, C. Ji, X. Jiang, K. Li, Y. Li and Y. Wang, *Chem. Commun.*, 2012, **48**, 10627–10629.
47 X. Zhao, C. Piliego, B. Kim, D. A. Poulsen, B. Ma, D. A. Unruh and J. M. J. Fréchet, *Chem. Mater.*, 2010, **22**, 2325–2332.
48 N. Cho, K. Song, J. K. Lee and J. Ko, *Chem.–Eur. J.*, 2012, **18**, 11433–11439.
49 C. B. Nielsen, J. Arnbjerg, M. Johnsen, M. Jørgensen and P. R. Ogilby, *J. Org. Chem.*, 2009, **74**, 9094–9104.
50 E. Preis and U. Scherf, *Macromol. Rapid Commun.*, 2006, **27**, 1105–1109.
51 H. Bronstein, J. M. Frost, A. Hadipour, Y. Kim, C. B. Nielsen, R. S. Ashraf, B. P. Rand, S. Watkins and I. McCulloch, *Chem. Mater.*, 2013, **25**, 277–285.
52 D. Dang, W. Chen, R. Yang, W. Zhu, W. Mammo and E. Wang, *Chem. Commun.*, 2013, **49**, 9335–9337.
53 R. Kroon, R. Gehlhaar, T. T. Steckler, P. Henriksson, C. Müller, J. Bergqvist, A. Hadipour, P. Heremans and M. R. Andersson, *Sol. Energy Mater. Sol. Cells*, 2012, **105**, 280–286.
54 Y. Zhang, S.-C. Chien, K.-S. Chen, H.-L. Yip, Y. Sun, J. A. Davies, F.-C. Chen and A. K. Y. Jen, *Chem. Commun.*, 2011, **47**, 11026–11028.
55 S. C. Price, A. C. Stuart, L. Yang, H. Zhou and W. You, *J. Am. Chem. Soc.*, 2011, **133**, 4625–4631.
56 H. Zhou, L. Yang, A. C. Stuart, S. C. Price, S. Liu and W. You, *Angew. Chem., Int. Ed.*, 2011, **123**, 3051–3054.
57 M. C. Scharber, D. Wuhlbacher, M. Koppe, P. Denk, C. Waldauf, A. J. Heeger and C. L. Brabec, *Adv. Mater.*, 2006, **18**, 789–794.
58 M. M. Wienk, J. M. Kroon, W. J. H. Verhees, J. Knol, J. C. Hummelen, P. A. van Hal and R. A. J. Janssen, *Angew. Chem., Int. Ed.*, 2003, **115**, 3493–3497.
59 P. W. M. Blom, V. D. Mihailetchi, L. J. A. Koster and D. E. Markov, *Adv. Mater.*, 2007, **19**, 1551–1566.
60 T.-Y. Chu, J. Lu, S. Beaupré, Y. Zhang, J.-R. Pouliot, J. Zhou, A. Najari, M. Leclerc and Y. Tao, *Adv. Funct. Mater.*, 2012, **22**, 2345–2351.
61 J. J. M. Halls, C. A. Walsh, N. C. Greenham, E. A. Marseglia, R. H. Friend, S. C. Moratti and A. B. Holmes, *Nature*, 1995, **376**, 498–500.